NANO LETTERS

pubs.acs.org/NanoLett Letter

Coexisting Magnetism, Ferroelectric, and Ferrovalley Multiferroic in Stacking-Dependent Two-Dimensional Materials

Wei Xun, Chao Wu, Hanbo Sun, Weixi Zhang, Yin-Zhong Wu, and Ping Li*

Cite This: *Nano Lett.* 2024, 24, 3541−3547 Read Online

ACCESS | Metrics & More | Article Recommendations | Supporting Information

ABSTRACT: Two-dimensional (2D) multiferroic materials have widespread application prospects in facilitating the integration and miniaturization of nanodevices. However, the magnetic, ferroelectric, and ferrovalley properties in one 2D material are rarely coupled. Here, we propose a mechanism for manipulating magnetism, ferroelectric, and valley polarization by interlayer sliding in a 2D bilayer material. Monolayer GdI_2 is a ferromagnetic semiconductor with a valley polarization of up to 155.5 meV. More interestingly, the magnetism and valley polarization of bilayer GdI_2 can be strongly coupled by sliding ferroelectricity, making these tunable and reversible. In addition, we uncover the microscopic mechanism of the magnetic phase transition by a spin Hamiltonian and electron hopping between layers. Our findings offer a new direction for investigating 2D multiferroic devices with implications for next-generation electronic, valleytronic, and spintronic devices.

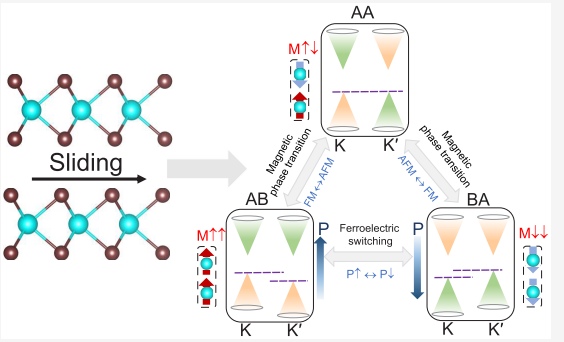

KEYWORDS: *two-dimensional multiferroic, sliding ferroelectricity, ferrovalley, magnetic phase transition, d-orbital hopping*

Two-dimensional (2D) van der Waals (vdW) materials are burgeoning as some of the top candidates due to their various structures, miniaturized dimensionality, and electronic engineering degrees of freedom, and they have highly tunable magnetic, electronic, and optical properties.[1−6] The weak interlayer vdW interaction also unleashes the flexibility to affect physical properties by vdW stacking. Recently, sliding ferroelectricity has originated from polar stacking of nonpolar monolayer transition metal dichalcogenides (TMDs)[7−9] and interlayer sliding in AlN and BN bilayers.[10,11] Besides, stacking orders effectively regulate the magnetic ground state, resulting in a magnetic phase transition, such as in the CrI_3[12] and $CrBr_3$[13] bilayers. More interestingly, the topological states can be tuned by the stacking order in a $MnBr_3$ bilayer.[14] Through interlayer sliding of 2D materials, Ma et al. proved in theory that $MnBi_2Te_4$,[15] Co_2CF_2,[16] $FeCl_2$,[17] etc., can realize a layer-polarized anomalous Hall effect (LPAHE). Additionally, the stacking order can effectively tune the intrinsic valley polarization of ferrovalley materials, such as YI_2[18] and $VSiGeP_4$.[19] These findings suggest that the stacking order has a profound effect on determining the crystal symmetry, reallocating spin and charge between neighboring layers, and thus regulating the strength of ferroelectric, magnetic, topological, and valley polarization properties.

Multiferroics, materials exhibiting coupled two or more ferroic orders (i.e., ferromagnetic, ferroelectric, ferroelastic, and ferrovalley), are especially interesting for next-generation electronic devices. At present, 2D multiferroic systems are often multiferroic heterostructures, such as $Cr_2Ge_2Te_6/In_2Se_3$,[20] $LaCl/In_2Se_3$,[21] and Cr_2COOH/Sc_2CO_2.[22] However, the heterostructure system will increase the difficulty of the fabrication device in experiments, which is disadvantageous to wider application. In contrast, if the 2D multiferroic material can be realized by vdW stacking order in the same kind of material, it becomes more attractive. It will realize highly flexible and controllable coupling of multiple ferroic orders. Therefore, 2D multiferroic materials will further promote application prospects in nanodevices.

In this work, we propose a new design of 2D multiferroics including magnetism, ferroelectric, and ferrovalley properties. Here we focus on the coupling and phase transition of magnetic, ferroelectric, and ferrovalley properties by the effect of stacking orders in bilayer GdI_2. First, we theoretically proposed that monolayer GdI_2 shows spontaneously sizable valley polarization, which is manipulated by switching magnetization. Then, we found that bilayer GdI_2 endows the coexistence of magnetism, ferroelectric, and ferrovalley properties, supporting the designed target for manipulating magnetism and valley polarization via ferroelectric switching by interlayer sliding. Moreover, we reveal the microscopic

Received: February 2, 2024
Revised: March 2, 2024
Accepted: March 4, 2024
Published: March 7, 2024

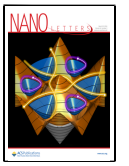

https://doi.org/10.1021/acs.nanolett.4c00597
Nano Lett. 2024, 24, 3541−3547

mechanism of the magnetic phase transition by a spin Hamiltonian and electron hopping between layers. The highly flexible tunable multiferroic in bilayer GdI_2 offers a practical way for designing advanced valleytronic and spintronic devices on account of the couplings between multiferroic orders.

The 2D multiferroic systems with the coexistence of magnetism, ferroelectrics, and ferrovalleys are established. Practically, for a monolayer system with intrinsically spontaneous valley polarization, it can realize multiferroic behavior by bilayer stacking and interlay sliding. As shown in Figure 1, the system realizes the mechanism of a 2D multiferroic with the coexistence of magnetism, ferroelectric, and ferrovalley properties. In AA stacking, the magnetic ground state is antiferromagnetic (AFM) coupling. Simultaneously, there is no spontaneous valley polarization and ferroelectric polarization in the system. When the AA stacking slides to AB or BA stacking, a magnetic phase transition from the AFM state to ferromagnetic (FM) state occurs, inducing spontaneous valley polarization and ferroelectric polarization (signed by dark gray arrows). Moreover, the AB and BA stacking can be transformed into each other by interlayer sliding, leading to a switch of the ferroelectric polarization between $+z$ and $-z$ axis directions.

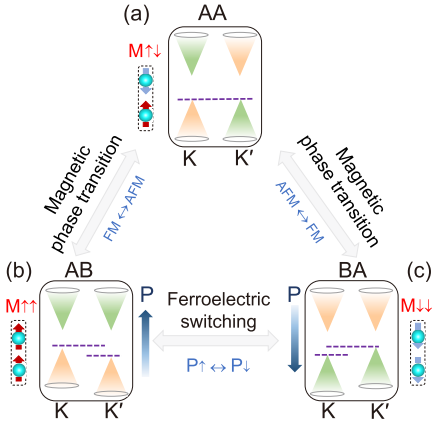

Figure 1. Illustration of the mechanism of a coexisting magnetic, ferroelectric, and ferrovalley multiferroic. (a) The magnetic ground state of AA stacking bilayer lattice is the AFM state, without spontaneous valley polarization. On an AA stacking slide to AB stacking (b) or BA stacking (c), the magnetic ground state will switch to an FM state. Simultaneously, spontaneous valley polarization will be realized. The valley polarization can also be manipulated via ferroelectric switching in AB stacking (b) and BA stacking (c). Orange and light green cones represent spin-up and spin-down bands, respectively. Dark gray arrows denote ferroelectric polarization P.

Figure 2a exhibits the crystal structure of the monolayer GdI_2. The inversion symmetry is broken in the monolayer GdI_2. The in-plane lattice constant for the fully optimized species is 4.17 Å. Besides, in order to study the bonding characteristics of monolayer GdI_2, we calculated the electron localization function (ELF). As shown in Figure 2b, the electrons are mainly localized around the Gd and I atoms, while those are negligible between the atoms, showing typical ionic bonding for all of the bonds. In addition, to evaluate the stability of the monolayer GdI_2, we calculate the phonon dispersion spectrum. As shown in Figure 2c, the absence of imaginary modes along the high-symmetry lines confirms the dynamic stability of monolayer GdI_2. Moreover, we calculated the formation energy, which is −11.140 eV. It indicates that GdI_2 is easily prepared.

In order to make sure of the magnetic ground state of monolayer GdI_2, a rectangular supercell is constructed (see Figure S1). The energy difference $\Delta E = E_{FM} - E_{AFM}$ between FM and AFM states is found to be −266 meV, meaning that the magnetic ground state of monolayer GdI_2 is the FM state. However, the successful preparations of 2D magnetic $Cr_2Ge_2Te_6$[3] and CrI_3[4] reveal that the magnetic anisotropy energy (MAE) plays an important role in the stability of magnetic order. Therefore, we investigate the MAE, defined as the energy difference $MAE = E_{001} - E_{100}$ between the magnetic moments along [001] and [100]. The MAE is 0.777 meV per

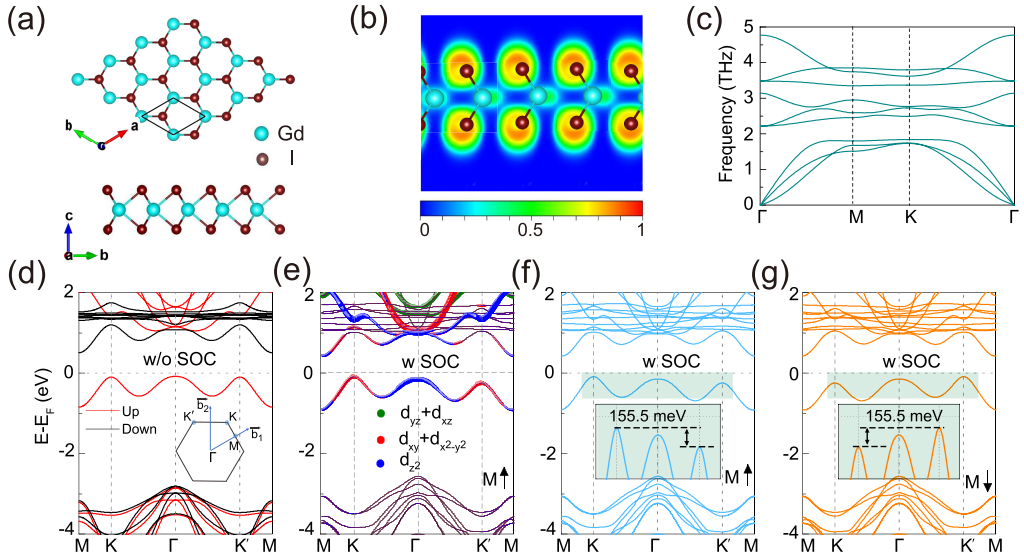

Figure 2. (a) Crystal structures of monolayer GdI_2 from top and side views. (b) Electron localization function of monolayer GdI_2. (c) The calculated phonon spectrum along the high symmetry. (d) Spin-polarized band structure of monolayer GdI_2. (e) The orbital-resolved band structure with consideration of SOC. (f, g) The band structures with consideration of SOC of magnetic moments along $+z$ (f) and $-z$ (g) axis directions, respectively.

https://doi.org/10.1021/acs.nanolett.4c00597
Nano Lett. 2024, 24, 3541−3547

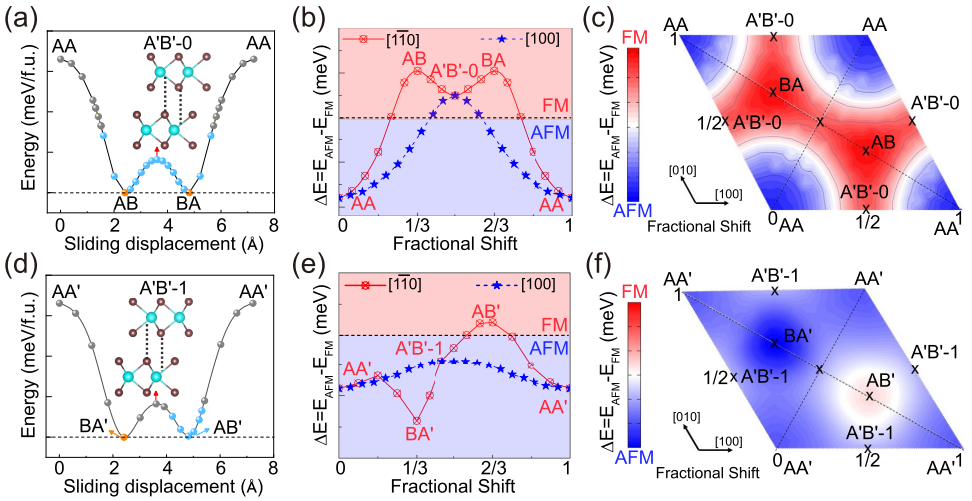

Figure 3. Sliding energy barrier between upper and lower layers of (a) AA stacking and (d) AA′ stacking bilayer GdI_2. The gray and blue balls indicate that the magnetic ground states are AFM and FM states, respectively. The orange balls represent the energy minima. The energy difference between interlayer AFM and FM states as a function of interlayer translation along [1$\bar{1}$0] (solid red line) and [100] (dotted blue line) direction for AA stacking (b) and AA′ stacking (e) bilayer GdI_2. The full space of lateral shifts for AA stacking (c) and AA′ stacking (f) bilayer GdI_2. The positive or negative regions represent FM or AFM states, respectively.

unit cell, standing for the magnetization along the x axis. For the monolayer GdI_2, a magnetic field ($H = -\frac{4}{3}\frac{K}{\mu_0 M}$) of 3.58 T is needed to tune the direction of magnetization from the x to z axis.

Next, we focus on the band structures and associated valley properties of monolayer GdI_2. As shown in Figure 2d, it is an indirect semiconductor in the absence of spin−orbit coupling (SOC); the valence band maximum (VBM) belongs to the spin-up band, located at the high-symmetry K and K′ points. While the conduction band minimum (CBM) is contributed by the spin-down band, located at the high-symmetry Γ point. Note that the K and K′ valleys of VBM are energetically degenerate. When the SOC is switched on, as shown in Figure 2e,f, the degeneracy between K and K′ valleys is broken. The valley splitting is 155.5 meV in monolayer GdI_2, which is larger than those in VSe_2 (90 meV),[23,24] $VSiXN_4$ (~70 meV),[25] $MoTe_2$/EuO (~20 meV),[26] and other ferrovalley materials. More fascinatingly, when the magnetization direction is switched from the $+z$ axis to the $-z$ axis, the valley polarization can be effectively tuned (see Figure 2g). From the orbital-resolved band structure (see Figure 2e and Figure S2), the VBM bands are mainly dominated by Gd d_{xy} and $d_{x^2-y^2}$ orbitals, while the CBM bands are contributed by Gd d_{xy}, $d_{x^2-y^2}$, and d_{z^2} orbitals. Moreover, we calculate the valley polarization of U values from 2.5 to 5 eV. As shown in Figure S3, we can clearly observe that the valley polarization increases first and then decreases. However, the range of variation is very small, only 0.5 meV.

To understand the microscopic mechanism in the valley splitting of valence bands, we use an effective Hamiltonian model to describe the physical nature of valley polarization induced by the SOC effect. Taking the SOC effect as the perturbation term

$$\hat{H}_{SOC} = \lambda \hat{L}\cdot\hat{S} = \hat{H}^0_{SOC} + \hat{H}^1_{SOC} \tag{1}$$

where $\hat{L}$ and $\hat{S}$ are orbital angular and spin angular operators, respectively. $\hat{H}^0_{SOC}$ denotes the interaction between the same spin states, while $\hat{H}^1_{SOC}$ represents the interaction between the opposite spin states. Since the VBM is contributed by the spin-up band, therefore, the term $\hat{H}^1_{SOC}$ can be neglected. For $\hat{H}^0_{SOC}$, it can be written by the polar angles[27]

$$\hat{H}^0_{SOC} = \lambda \hat{S}z'\left(\hat{L}_z \cos\theta + \frac{1}{2}\hat{L}_+ e^{-i\phi}\sin\theta + \frac{1}{2}\hat{L}_- e^{+i\phi}\sin\theta\right) \tag{2}$$

When the magnetization of monolayer GdI_2 is along the out-of-plane direction, $\theta = \phi = 0°$; therefore, the $\hat{H}^0_{SOC}$ term can be simplified as

$$\hat{H}^0_{SOC} = \lambda \hat{S}_z \hat{L}_z \tag{3}$$

Considering the C_3 symmetry and the contribution of the orbital, we chose $|\psi^\tau_v\rangle = \frac{1}{\sqrt{2}}(|d_{xy}\rangle + i\tau|d_{x^2-y^2}\rangle)\otimes|\uparrow\rangle$ as the orbital basis functions for the VBM, where $\tau = \pm 1$ represent the valley index corresponding to K/K′. The energy of the K and K′ valleys for the VBM can be written as $E^\tau_v = \langle\psi^\tau_v|\hat{H}^0_{SOC}|\psi^\tau_v\rangle$. Then, the valley splitting in the valence band can be written as

$$E^K_v - E^{K'}_v = i\langle d_{xy}|\hat{H}^0_{SOC}|d_{x^2-y^2}\rangle - i\langle d_{x^2-y^2}|\hat{H}^0_{SOC}|d_{xy}\rangle \approx 4\beta \tag{4}$$

where $\hat{L}_z|d_{xy}\rangle = -2i\hbar|d_{x^2-y^2}\rangle$, $\hat{L}_z|d_{x^2-y^2}\rangle = 2i\hbar|d_{xy}\rangle$, and $\beta = \lambda\langle d_{x^2-y^2}|\hat{S}z'|d_{x^2-y^2}\rangle$. The analytical result proves that the valley splitting of valence band is consistent with our DFT calculations ($E^K_v - E^{K'}_v$ = 155.5 meV).

Layer stacking of 2D magnetic materials likely induces intriguing physical phenomena, which differ from those of the monolayer materials.[12−17,28] Here, we investigate novel physical behaviors of bilayer GdI_2 by stacking orders. Six typical stacking structures, AA, AB, BA, AA′, AB′, and BA′, are shown in Figure S4. The AA stacking bilayer GdI_2 is constructed by primitively placing one layer on top of the other layer. Therefore, the AA stacking layer GdI_2 has mirror

https://doi.org/10.1021/acs.nanolett.4c00597
Nano Lett. 2024, 24, 3541−3547

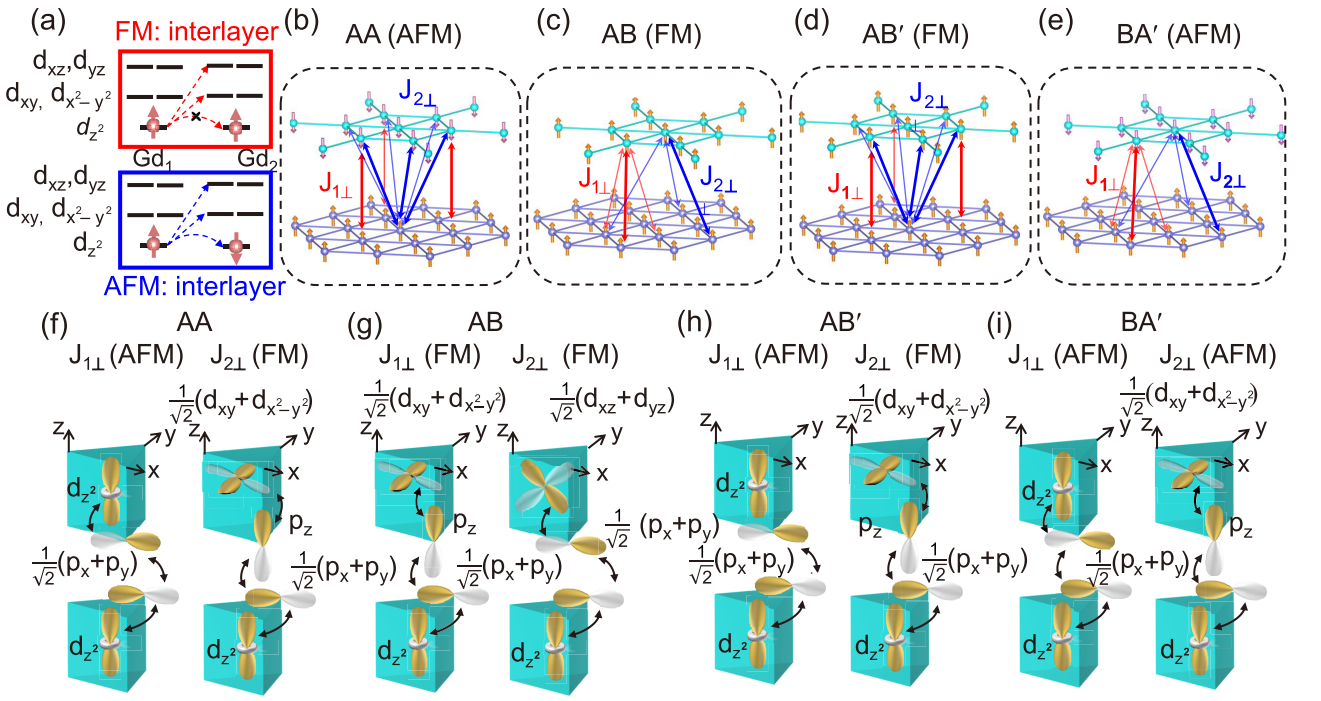

Figure 4. (a) Schematic of the orbital dependent interlayer exchange interactions. The hopping from d_{z^2}−d_{z^2} is allowed in the AFM exchange, whereas it is prohibited in the FM exchange. (b−e) The interlayer Gd nearest neighbor and second-nearest neighbor correspond to $J_{1\perp}$ (red) and $J_{2\perp}$ (blue) for AA (b), AB (c), AB′ (d), and BA′ (e) stacking, respectively. (f−i) Schematics of supersuperexchange for AA (f), AB (g), AB′ (h), and BA′ (i) stacking, respectively.

symmetry between the two layers about the *xy* plane. AB and BA stacking are obtained by sliding $t_{1\parallel}[\frac{2}{3}, \frac{1}{3}, 0]$ and $t_{1\parallel}[\frac{1}{3}, \frac{2}{3}, 0]$ of AA stacking, respectively. However, the AA′, stacking can be realized by rotating the upper layer 180° of AA stacking about the xy plane. AA′, stacking could be transformed into the AB′, and BA′, stacking by by sliding $t_{1\parallel}[\frac{2}{3}, \frac{1}{3}, 0]$ and $t_{1\parallel}[\frac{1}{3}, \frac{2}{3}, 0]$, respectively.

The sliding energy barriers of two kinds of stacking patterns are investigated to acquire ground-state stacking configurations. As shown in Figure 3a, for the one kind of stacking, AB and BA stackings exhibit the lowest energy, while the AA stacking has the highest energy. The transition of AB stacking into BA stacking requires overcoming an energy barrier of 16.42 meV. For the other kinds of stacking (see Figure 3d), BA′ stacking shows the lowest energy, while the energy of AB′ stacking is 0.75 meV larger than that of BA′ stacking. The above analysis shows that AB, BA, and BA′ are stable for bilayer GdI_2. To understand the effect of stacking on magnetism, we calculate the energy difference between the interlayer AFM and FM states, as shown in Figure 3b,e for the kinds of AA and AA′ stackings, respectively. Seeing is believing, as the magnitude of interlayer magnetic interaction for the kind of AA stacking is stronger than that of the kind of AA′ stacking. First, for the kind of AA stacking, we find that the AA stacking strongly prefers AFM, and the corresponding interlayer exchange energy is about −1.794 meV (see Figure S5). On the contrary, the interlayer exchange energy of AB and BA stackings is 1.046 meV (see Figure S5); this indicates that the magnetic phase transition occurs from AA stacking sliding to AB or BA stacking. Furthermore, for the other (the kind of AA′ stacking), the vicinity of AB′ stacking prefers the FM state, while the other regions favor AFM coupling. In a word, it indicates a strong coupling between magnetism and stacking order.

Are there other intriguing stacking orders? In order to answer the question, we calculated the interlayer exchange energy of the kinds of AA and AA′ stackings for the entire 2D space of lateral shifts. We chose a 6 × 6 grid to employ the lateral shifts. Figure 3c,f shows the energy difference between interlayer AFM and FM states for the full 2D space of lateral shifts. One can see that the magnetic ground state switches between the AFM and FM states as the interlayer stacking order changes. Moreover, the D_{3h}-symmetric AA stacking prefers the AFM state. However, the magnetic interlayer interaction becomes FM coupling for AB and BA stackings, when the D_{3h} symmetry breakd the *xy* mirror symmetry (C_{3v}). It is well-known that the broken *xy* mirror symmetry for the D_{3h} point group induces the out-of-plane electric polarization *P*.[10] As shown in Figure S6, the electrostatic potential difference with the positive (negative) discontinuity $\Delta\Phi$ = 22.86 (−22.86) meV is generated between the vacuum levels of upper and lower layers, which clearly proves that the spontaneous *P* is produced along the +*z* (−*z*) axis in the AB (BA) stacking bilayer. The electric polarization value of AB stacking bilayer GdI_2 is up to 3.68×10^{-12} C/m. The AB and BA stacking bilayers can realize reciprocal transformation by interlayer sliding; therefore, we came to the conclusion that the sliding ferroelectric exists in bilayer GdI_2, which can also be confirmed from the general theory of bilayer sliding ferroelectricity.[29] It indicates that the magnetic ground state can effectively be tuned by the sliding ferroelectric. Note that the kind of AA′ stacking does not have spontaneous polarization due to the 180° rotation between two layers inducing the out-of-plane polarization to cancel (see Figure S7).

https://doi.org/10.1021/acs.nanolett.4c00597
Nano Lett. 2024, 24, 3541−3547

Table 1. Interlayer Distance of Nearest Neighbors and Second-Nearest Neighbors between Gd Atoms, the Number of Magnetic Exchange Interactions per Unit Cell in Brackets, the Calculated Heisenberg Exchange Parameters, and the Energy Difference between Interlayer AFM and FM States for the Different Stacking Configurations

stacking	Gd−Gd NN (Å)	Gd−Gd second-NN (Å)	$J_{1\perp}$ (meV)	$J_{2\perp}$ (meV)	$J_{\parallel}$ (meV)	ΔE (meV)
AA	8.139 [1]	9.145 [6]	0.243	−0.003	−8.253	−1.794
AB	7.888 [3]	8.922 [3]	−0.036	−0.007	−8.242	1.046
AB′	7.505 [1]	8.586 [6]	0.002	−0.004	−8.235	0.206
BA′	7.915 [3]	8.946 [3]	0.066	−0.008	−8.256	−1.403

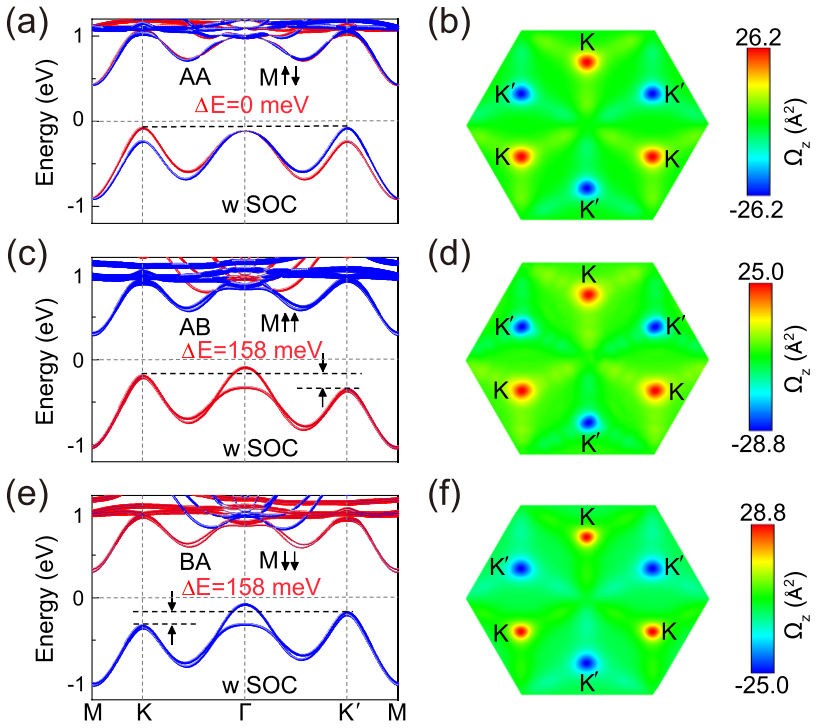

Figure 5. Spin-resolved band structures and Berry curvatures of AA (a, b), AB (c, d), and BA (e, f) stacking bilayer GdI_2 with consideration of the SOC effect.

To understand the microscopic mechanism of magnetic coupling, we consider the simple spin Hamiltonian

$$H = E_0 + \sum_{i,j} J_{\parallel} S_i \cdot S_j + \sum_{i,k} J_{1\perp} S_i \cdot S_k + \sum_{i,l} J_{2\perp} S_i \cdot S_l \quad (5)$$

where E_0 is the ground state energy independent of the spin configurations. S_i, S_j, S_k, and S_l denote the magnetic moments at sites i, j, k, and l, respectively. $J_{\parallel}$, $J_{1\perp}$, and $J_{2\perp}$ represent the intralayer, nearest-neighbor (NN) interlayer, and second-nearest-neighbor (second-NN) interlayer Gd−Gd exchange interactions, respectively (see Figure 4). The details for the calculation of Heisenberg exchange parameters based on the above spin Hamiltonian and total energy calculations employing DFT are shown in the Supporting Information and Table 1. The intralayer exchange is strong FM coupling (∼−8.25 meV), while the interlayer exchange interaction depends on the stacking order.

Since the Gd atoms in GdI_2 are in a $4f^7 5d^1$ electronic configuration (see Figure S2), according to the Pauli exclusion principle and Hund's rule, the electron configuration will half-fill the f and d_{z^2} orbitals. In the trigonal-prismatic crystal field, the schematic illustrations of Gd-5d and Gd-4f orbital splitting are shown in Figure S2b. According to the energy minimizing principle of hopping, the magnetic exchange between the two layers is determined by the d orbital hopping. Figure 4a exhibits a schematic of the FM and AFM exchange interactions between Gd atoms in the interlayer. The hopping between d_{z^2} and d_{z^2} is prohibited for the FM spin configuration (red), while it is allowed for the AFM spin configuration (blue). Hence, d_{z^2}-d_{z^2} hybridization results in AFM. On the other hand, hopping of from d_{z^2}−d_{xy}/ $d_{x^2-y^2}$ and d_{z^2}−d_{xz}/d_{yz} gives rise to an exchange coupling that is overwhelmingly FM from the viewpoint of the local Hund coupling.[30,31] The interlayer Gd−Gd exchange interactions of all stackings are mediated via hybridization between the I-p orbitals. Therefore, the nature of interlayer exchange interaction is supersuperexchange. The magnetism of stacking order dependence derives from the competition between the orbital hybridizations of different interlayers.

In the following, we take four typical stacking patterns as examples for detailed analysis. For the AA stacking, Figure 4b shows the interlayer NN exchange interaction of Gd−Gd $J_{1\perp}$ (red) and second-NN exchange interaction of Gd−Gd $J_{2\perp}$ (blue) for AA stacking. As shown in Figure 4f, $J_{1\perp}$ predominates via virtual excitations between Gd half-filled d_{z^2} orbitals, causing an AFM coupling.[32] By contrast, $J_{2\perp}$ is dominated by virtual excitations between Gd half-filled d_{z^2} and the empty d_{xy}/ $d_{x^2-y^2}$ orbitals, leading to the FM coupling. As listed in Table 1, although AA stacking has only one $J_{1\perp}$ bond

https://doi.org/10.1021/acs.nanolett.4c00597
Nano Lett. 2024, 24, 3541−3547

and six $J_{2\perp}$ bonds per unit cell, $J_{1\perp}$ is much larger than $J_{2\perp}$. Therefore, the NN interlayer AFM coupling dominates the second-NN interlayer FM coupling, resulting in the AFM state for AA stacking of GdI_2. For the AB stacking, the sliding of one layer of $t_{1\parallel}[\frac{2}{3}, \frac{1}{3}, 0]$ relative to the other breaks the interlayer hybridization between I-p electrons and produces new ones. As shown in Figure 4c, the NN ligancy number is increased compared with the AA stacking, and the second-NN ligancy number is decreased (see Table 1). Simultaneously, the virtual excitations of $J_{1\perp}$ become between Gd half-filled d_{z^2} and the empty $d_{xy}/d_{x^2-y^2}$ orbitals, indicating the FM coupling. While $J_{2\perp}$ is dominated by virtual excitations between Gd half-filled d_{z^2} and the empty d_{xz}/d_{yz} orbitals, contributing also to the FM coupling. As a result, the magnetic ground state becomes an FM state. Although the coordination number of AB′ (BA′) stacking is consistent with AA (AB) stacking, they exhibit opposite magnetic ground states. It originates from the symmetry difference (see Figure S4, Figure 4b−i, and Table 1).

Stacking orders induce not only the changes of magnetic ground state and ferroelectric polarization but also the transformation of valley polarization due to the different symmetries. As shown in Figure 5a and Figure S8a−d, the band structures of AA stacking bilayer GdI_2 are investigated based on the AFM (M↑↓) magnetic ground state. In the absence of SOC, spin-up and spin-down bands are degenerate (Figure S8a). When the SOC is switched on, as shown in Figure 5a, the degeneracy of spin-up and spin-down bands disappears. In detail, we focus on the valence band. The spin-up band shifts above the spin-down band in the K valley, while the spin-up band shifts below the spin-down band in the K′ valley. More interestingly, the spin-up and spin-down bands of K and K′ valleys are degenerate in energy. From the orbital-resolved band structure (see Figure S8b), the VBM bands are also dominated by Gd d_{xy} and $d_{x^2-y^2}$ orbitals; this is consistent with monolayer GdI_2. Moreover, as shown in Figure 5b, the Berry curvatures of K and K′ valleys have equal magnitudes and opposite signs (26.2 Å^2 for the K point and −26.2 Å^2 for the K′ point).

When the AA stacking slides to AB stacking, the degeneracy of spin up and spin down bands disappears in the absence of SOC (see Figure S8e). It originates from the magnetic ground state from an AFM state transition to an FM state. When the SOC is included, as shown in Figure 5c, it produces a valley polarization of 158 meV. It indicates that the interlayer sliding induces the out-of-plane ferroelectric polarization simultaneously, leading to the magnetic phase transition and valley polarization. Due to the valley polarization generation, as shown in Figure 5d, the Berry curvature magnitudes of K and K′ valleys are no longer equal, and the signs are still opposite (25.0 Å^2 for K point and −28.8 Å^2 for K′ point). On further slipping to BA stacking, the valley polarization is reversed by the ferroelectric switching, as shown in Figure 5e. Meanwhile, the Berry curvatures of K and K′ valleys change to 28.8 and −25.0 Å^2, respectively (see Figure 5f). In addition, the other stacking also produces intriguing coupling of magnetic, ferroelectric, and ferrovalley orders (Figure S9).

In conclusion, we propose a mechanism to realize coexisting magnetism and ferroelectric and ferrovalley multiferroic properties in 2D materials. The mechanism is proved in bilayer GdI_2. By transformation of the interlayer stacking order, one can regulate the magnetic ground state, ferroelectric polarization, and valley polarization for bilayer GdI_2. The magnetic ground state of AA stacking is the AFM state with the degeneracy at the VBM of K and K′ valleys. As the AA stacking slides to AB (BA) stacking, its spontaneous valley polarization occurs due to the magnetic ground state transforming from the AFM to the FM state. The AB stacking changes to the BA stacking state by interlayer sliding, and the ferroelectric polarization and valley polarization are switched. Moreover, we reveal the microscopic mechanism of a magnetic phase transition by a spin Hamiltonian and electron hopping between layers. Our work offers not only a novel 2D multiferroic material but also an efficient means to tune magnetic, ferroelectric, and ferrovalley properties.

■ ASSOCIATED CONTENT

Supporting Information

The Supporting Information is available free of charge at https://pubs.acs.org/doi/10.1021/acs.nanolett.4c00597.

Details of the calculation methods, spin Hamiltonian model, spin charge density, orbital-resolved band structures, the effect of U value on valley polarization, stacking structures of bilayer GdI_2, the energy difference between interlayer AFM and FM for a bilayer, the plane-averaged electrostatic potential, and band structures for bilayer GdI_2 (PDF)

■ AUTHOR INFORMATION

Corresponding Author

Ping Li − *State Key Laboratory for Mechanical Behavior of Materials, Center for Spintronics and Quantum System, School of Materials Science and Engineering, Xi'an Jiaotong University, Xi'an, Shaanxi 710049, People's Republic of China; State Key Laboratory for Surface Physics and Department of Physics, Fudan University, Shanghai 200433, China;* orcid.org/0000-0001-8285-8921; Email: pli@xjtu.edu.cn

Authors

Wei Xun − *State Key Laboratory for Mechanical Behavior of Materials, Center for Spintronics and Quantum System, School of Materials Science and Engineering, Xi'an Jiaotong University, Xi'an, Shaanxi 710049, People's Republic of China; Faculty of Electronic Information Engineering, Huaiyin Institute of Technology, Huaian 223003, People's Republic of China;* orcid.org/0000-0001-5299-3786

Chao Wu − *State Key Laboratory for Mechanical Behavior of Materials, Center for Spintronics and Quantum System, School of Materials Science and Engineering, Xi'an Jiaotong University, Xi'an, Shaanxi 710049, People's Republic of China*

Hanbo Sun − *State Key Laboratory for Mechanical Behavior of Materials, Center for Spintronics and Quantum System, School of Materials Science and Engineering, Xi'an Jiaotong University, Xi'an, Shaanxi 710049, People's Republic of China*

Weixi Zhang − *Department of Physics and Electronic Engineering, Tongren University, Tongren 554300, People's Republic of China*

Yin-Zhong Wu − *School of Physical Science and Technology, Suzhou University of Science and Technology, Suzhou 215009, People's Republic of China;* orcid.org/0000-0002-0463-9202

Complete contact information is available at:

https://doi.org/10.1021/acs.nanolett.4c00597
Nano Lett. 2024, 24, 3541−3547

https://pubs.acs.org/10.1021/acs.nanolett.4c00597

Notes

The authors declare no competing financial interest.

■ ACKNOWLEDGMENTS

This work was supported by the National Natural Science Foundation of China (Grant No. 12004295). P.L. thanks China's Postdoctoral Science Foundation funded project (Grant No. 2022M722547), the Fundamental Research Funds for the Central Universities (xxj03202205), and the Open Project of State Key Laboratory of Surface Physics (No. KF2022_09).

■ REFERENCES

(1) Novoselov, K. S.; Geim, A. K.; Morozov, S. V.; Jiang, D.; Zhang, Y.; Dubonos, S. V.; Grigorieva, I. V.; Firsov, A. A. Electric Field Effect in Atomically Thin Carbon Films. *Science* **2004**, *306*, 666.

(2) Cao, T.; Wang, G.; Han, W.; Ye, H.; Zhu, C.; Shi, J.; Niu, Q.; Tan, P.; Wang, E.; Liu, B.; Feng, J. Valley-selective circular dichroism of monolayer molybdenum disulphide. *Nat. Commun.* **2012**, *3*, 887.

(3) Gong, C.; Li, L.; Li, Z.; Ji, H.; Stern, A.; Xia, Y.; Cao, T.; Bao, W.; Wang, C.; Wang, Y.; Qiu, Z. Q.; Louie, S. G.; Xia, J.; Zhang, X. Discovery of intrinsic ferromagnetism in two-dimensional van der Waals crystals. *Nature* **2017**, *546*, 265.

(4) Huang, B.; Clark, G.; Navarro-Moratalla, E.; Klein, D. R.; Cheng, R.; Seyler, K. L.; Zhong, D.; Schmidgll, E.; McGuire, M. A.; Cobden, D. H.; Yao, W.; Xiao, D.; Jarillo-Herrero, P.; Xu, X. Layer-dependent ferromagnetism in a van der Waals crystal down to the monolayer limit. *Nature* **2017**, *546*, 270.

(5) Li, W.; Qian, X.; Li, J. Phase transitions in 2D materials. *Nat. Rev. Mater.* **2021**, *6*, 829.

(6) Li, P.; Zhou, X. S.; Guo, Z. X. Intriguing magnetoelectric effect in two-dimensional ferromagnetic/perovskite oxide ferroelectric heterostructure. *npj Comput. Mater.* **2022**, *8*, 20.

(7) Fei, Z.; Zhao, W.; Palomaki, T. A.; Sun, B.; Miller, M. K.; Zhao, Z.; Yan, J.; Xu, X.; Cobden, D. H. Ferroelectric switching of a two-dimensional metal. *Nature* **2018**, *560*, 336.

(8) Xiao, J.; Wang, Y.; Wang, H.; Pemmaraju, C. D.; Wang, S.; Muscher, P.; Sie, E. J.; Nyby, C. M.; Devereaux, T. P.; Qian, X.; Zhang, X.; Lindenberg, A. M. Berry curvature memory through electrically driven stacking transitions. *Nat. Phys.* **2020**, *16*, 1028.

(9) Wang, X.; Yasuda, K.; Zhang, Y.; Liu, S.; Watanabe, K.; Taniguchi, T.; Hone, J.; Fu, L.; Jarillo-Herrero, P. Interfacial ferroelectricity in rhombohedral-stacked bilayer transition metal dichalcogenides. *Nat. Nanotechnol.* **2022**, *17*, 367.

(10) Li, L.; Wu, M. Binary compound bilayer and multilayer with vertical polarizations: two-dimensional ferroelectrics, multiferroics, and nanogenerators. *ACS Nano* **2017**, *11*, 6382.

(11) Yasuda, K.; Wang, X.; Watanabe, K.; Taniguchi, T.; Jarillo-Herrero, P. Stacking-engineered ferroelectricity in bilayer boron nitride. *Science* **2021**, *372*, 1458.

(12) Sivadas, N.; Okamoto, S.; Xu, X.; Fennie, C. J.; Xiao, X. Stacking-Dependent Magnetism in Bilayer CrI_3. *Nano Lett.* **2018**, *18*, 7658.

(13) Chen, W.; Sun, Z.; Wang, Z.; Gu, L.; Xu, X.; Wu, S.; Gao, C. Direct observation of van der Waals stacking-dependent interlayer magnetism. *Sicence* **2019**, *366*, 983.

(14) Li, X.; Xu, X.; Zhou, H.; Jia, H.; Wang, E.; Fu, H.; Sun, J. T.; Meng, S. Tunable topological states in stacked chern insulator bilayers. *Nano Lett.* **2023**, *23*, 2839.

(15) Peng, R.; Zhang, T.; He, Z.; Wu, Q.; Dai, Y.; Huang, B.; Ma, Y. Intrinsic layer-polarized anomalous Hall effect in bilayer $MnBi_2Te_4$. *Phys. Rev. B* **2023**, *107*, 085411.

(16) Feng, Y.; Dai, Y.; Huang, B.; Kou, L.; Ma, Y. Layer Hall Effect in Multiferroic Two-Dimensional Materials. *Nano Lett.* **2023**, *23*, 5367.

(17) Zhang, T.; Xu, X.; Guo, J.; Dai, Y.; Ma, Y. Layer-Polarized Anomalous Hall Effects from Inversion-Symmetric Single-Layer Lattices. *Nano Lett.* **2024**, *24*, 1009.

(18) Wu, Y.; Tong, J.; Deng, L.; Luo, F.; Tian, F.; Qin, G.; Zhang, X. Coexisting Ferroelectric and Ferrovalley Polarizations in Bilayer Stacked Magnetic Semiconductors. *Nano Lett.* **2023**, *23*, 6226.

(19) Li, Y. Q.; Zhang, X.; Shang, X.; He, Q. W.; Tang, D. S.; Wang, X. C.; Duan, C. G. Magnetic and Ferroelectric Manipulation of Valley Physics in Janus Piezoelectric Materials. *Nano Lett.* **2023**, *23*, 10013.

(20) Gong, C.; Kim, E. M.; Wang, Y.; Lee, G.; Zhang, X. Multiferroicity in atomic van der Waals heterostructures. *Nat. Commun.* **2019**, *10*, 2657.

(21) Sun, W.; Wang, W.; Li, H.; Zhang, G.; Chen, D.; Wang, J.; Cheng, Z. Controlling bimerons as skyrmion analogues by ferroelectric polarization in 2D van der Waals multiferroic heterostructures. *Nat. Commun.* **2020**, *11*, 5930.

(22) Li, P.; Wu, C.; Peng, C.; Yang, M.; Xun, W. Multifield tunable valley splitting in two-dimensional MXene Cr_2COOH. *Phys. Rev. B* **2023**, *108*, 195424.

(23) Tong, W. Y.; Gong, S. J.; Wan, X.; Duan, C. G. Concepts of ferrovalley material and anomalous valley Hall effect. *Nat. Commun.* **2016**, *7*, 13612.

(24) Li, P.; Liu, B.; Chen, S.; Zhang, W. X.; Guo, Z. X. Progress on two-dimensional ferrovalley materials. *Chin. Phys. B* **2024**, *33*, 017505.

(25) Li, P.; Yang, X.; Jiang, Q. S.; Wu, Y. Z.; Xun, W. Built-in electric field and strain tunable valley-related multiple topological phase transitions in $VSiXN_4$ (X = C, Si, Ge, Sn, Pb) monolayers. *Phys. Rev. Mater.* **2023**, *7*, 064002.

(26) Zhang, A.; Gong, Z.; Zhu, Z.; Pan, A.; Chen, M. Effects of the substrate-surface reconstruction and orientation on the spin valley polarization in $MoTe_2$/EuO. *Phys. Rev. B* **2020**, *102*, 155413.

(27) Wang, K.; Li, Y.; Mei, H.; Li, P.; Guo, Z. X. Quantum anomalous Hall and valley quantum anomalous Hall effects in two-dimensional d^0 orbital XY monolayers. *Phys. Rev. Mater.* **2022**, *6*, 044202.

(28) Zhang, C.; Guo, P.; Zhou, J. Tailoring bulk photovoltaic effects in magnetic sliding ferroelectric materials. *Nano Lett.* **2022**, *22*, 9297.

(29) Ji, J.; Yu, G.; Xu, C.; Xiang, H. J. General Theory for Bilayer Stacking Ferroelectricity. *Phys. Rev. Lett.* **2023**, *130*, 146801.

(30) Goodenough, J. B. Theory of the Role of Covalence in the Perovskite-Type Manganites [La, M(II)]MnO_3. *Phys. Rev.* **1955**, *100*, 564.

(31) Kanamori, J. Superexchange interaction and symmetry properties of electron orbitals. *J. Phys. Chem. Solids* **1959**, *10*, 87.

(32) Anderson, P. W. Antiferromagnetism. Theory of superexchange interaction. *Phys. Rev.* **1950**, *79*, 350.